hv photonics

IMPACT FACTOR 2.536

CITESCORE 2.3

Article

Time-Varying Engineered Reservoir for the Improved Estimation of Atom-Cavity Coupling Strength

Ye Xia, Weiming Guo and Zibo Miao

Special Issue

Quantum Optics: Science and Applications

Edited by

Dr. Hua-Lei Yin, Dr. Peng Xu and Dr. Jie Chen

MDPI

https://doi.org/10.3390/photonics10020157

photonics

MDPI

Article

Time-Varying Engineered Reservoir for the Improved Estimation of Atom-Cavity Coupling Strength

Ye Xia, Weiming Guo and Zibo Miao *

Harbin Institute of Technology, Shenzhen 518055, China
* Correspondence: miaozibo@hit.edu.cn

Abstract: In this paper, we consider the application of quantum reservoir engineering in quantum metrology. More precisely, we are concerned with a system setup where a sequence of atoms constructing the "time-varying" quantum reservoir interact, in turn, with the trapped field in a cavity through the Jaynes–Cummings Hamiltonian. In particular, we were able to manipulate the initial states of reservoir atoms in order to enhance estimation precision regarding the coupling strength between each atom and the cavity (the coupling strength between each atom and the cavity was assumed to be identical). The novelty of this work lies in alternately preparing the atoms at two different states in a pairwise manner, such that the cavity could converge into a squeezed state with photonic loss to the environment taken into account. The control scheme proposed here thus leads to higher precision compared to the previous work where reservoir atoms were initialized at the same state, which drove the cavity to a coherent state. Detailed theoretical analysis and numerical simulations are also provided. In addition, this system setup and the associated control scheme are easily implemented for quantum metrology, since no entanglement is required for the preparation of atom states, and the final cavity state can stay steady.

Keywords: quantum reservoir engineering; quantum metrology; squeezed states

Citation: Xia, Y.; Guo, W.; Miao, Z. Time-Varying Engineered Reservoir for the Improved Estimation of Atom-Cavity Coupling Strength. *Photonics* **2023**, *10*, 157. https://doi.org/10.3390/photonics10020157

Received: 13 December 2022
Revised: 30 January 2023
Accepted: 31 January 2023
Published: 2 February 2023

1. Introduction

During the past few decades, quantum metrology has been playing an important role in quantum science and technology. The procedure of quantum parameter estimation in general consists of three steps: preparing the probe state, letting the prepared probe state interact with the system (parameterization process), and measuring the final state [1,2]. These three parts all influence the estimation precision. There is established work concerning the preparation of the probe state and the selection of the measurement for the final state. The standard approach is to prepare the optimal probe state with the utilization of appropriate positive-operator-valued measurement (POVM) after the parameterization process [3–9]. In terms of optimizing the quantum state possessing the information of the parameter to be estimated, Carlton Morris Caves proposed that the squeezed vacuum state could help in improving the estimation precision in 1981 [10]. Since then, quantum properties in nonclassical states began to attract the attention of more researchers, leading to a boom in the development of quantum metrology. For example, it was proven both theoretically and experimentally that entangled coherent states [3,4], spin squeezed states [5,6] and two-mode squeezed vacuum states [7] can contribute to better estimation precision. On the other hand, in order to further improve estimation precision, control was introduced in the parameterization process, such as the gradient ascent pulse engineering (GRAPE) and the asynchronous advantage actor–critic algorithms aimed at optimally adjusting the parameterization process [11–13]. The Heisenberg limit can also not be surpassed by merely adding control terms to the Hamiltonian [14–16]. However, most of the above-mentioned works that involve adding control need coherent signals to be directly fed to the target

system, and entangled states are usually desired to enhance the estimation, which is indeed not simple to prepare in practice.

By contrast, quantum reservoir engineering provides an alternative way that can avoid adding real-time control directly to the target system. Rather, the target system is controlled indirectly by manipulating the reservoir. In this paper, the reservoir is composed of a sequence of atoms (qubits) that interact with the trapped field in a cavity (quantum harmonic oscillator) one after another through the Jaynes–Cummings Hamiltonian. The experimental background of this paper was first developed in [17]. Then, on the basis of this setup, it was proven that nonclassical states of the quantum harmonic oscillator could be stabilized through the interaction between the oscillator and the reservoir qubits [18,19], where it was demonstrated that the cavity could be stabilized at a coherent state with the atoms initialized at the same state, as shown in Figure 1. In particular, control signals do not need to be added to the oscillator, but the initial states of the reservoir qubits can be altered, such that the final state of the oscillator can be manipulated with the purpose of estimating the coupling strength between each qubit and the oscillator. This setting was used for quantum metrology in [20] where the qubits were initialized at an identical state; thus, the harmonic oscillator converged towards a coherent state with the averaged photon counting calculated to quantify the variance in coupling strength. Estimation precision was also proven to reach the Heisenberg limit in [20], where the root-mean-square fluctuation of the atom–cavity coupling strength was proportional to the square of the number of effective coupling atoms. Other reservoir engineering schemes are utilized to estimate qubit–oscillator coupling strength. For example, in [21], a quantum reservoir composed of N quantum harmonic oscillators interacting with the qubit was applied to estimate the coupling strength by calculating the quantum Fisher information (QFI) to quantify the precision. However, preparing the state of a qubit in [20] tended to be easier than preparing the joint state of N harmonic oscillators.

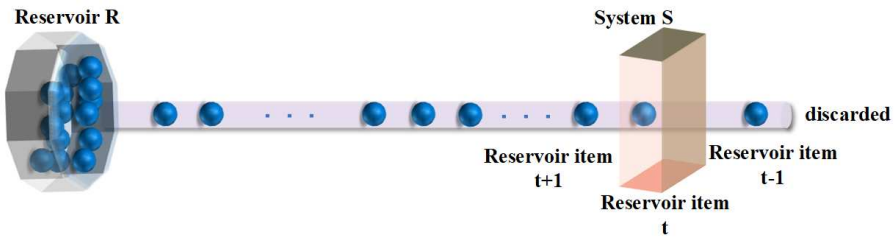

Figure 1. Framework of the quantum reservoir consisting of a sequence of qubits initialized at the same state.

By preparing the reservoir qubits at different states, which may initially involve entanglement, the harmonic oscillator could be stabilized at a squeezed coherent state with the squeezing strength determined by the initial qubit states [22,23]. Mainly inspired by [20,23], we aim to take advantage of a "time-varying" reservoir to enhance the estimation precision of qubit–oscillator coupling strength without entanglement involved in the reservoir qubits. The term "time-varying" means that the reservoir qubits are alternately initialized at two different states in a pairwise manner, as shown in Figure 2, but not initialized at the same state as that shown in Figure 1. In more concrete terms, reservoir qubits are initialized at $|\psi_{qred}\rangle, |\psi_{qblue}\rangle, |\psi_{qred}\rangle, |\psi_{qblue}\rangle, \cdots$ such that the harmonic oscillator can converge into a squeezed coherent state, since squeezed states enable us to significantly improve the estimation precision [24]. Furthermore, we took into account photonic loss to the environment in this paper; in [23], only the ideal case was considered. Qubits initialized under the scheme shown in Figure 2, steering the harmonic oscillator to a squeezed state, help in achieving higher precision than that of qubits initialized under the scheme shown in Figure 1, steering the harmonic oscillator to a coherent state in the absence of entanglement in the reservoir, which is not difficult to be realized in experiments. It is, thus, promising that the squeezed states stabilized by means of quantum reservoir engineering, as shown in Figure 2, can

be used to provide benefits to related works in the field of quantum information, such as [25–28].

The organization of this paper is as follows. In Section 2, we give the mathematical description of the system setup, especially concerning the consecutive pairs of separable "time-varying" reservoir qubits. In Section 3, we take into account photonic loss through the oscillator to the environment, providing the form of steady states together with the stability conditions. Furthermore, we prove that steering the oscillator to a squeezed state can give rise to a larger QFI compared to that of previous work where the oscillator was steered to a coherent state. This is also visualized and verified via simulation examples. Critical issues regarding our theoretical analysis and numerical simulation, together with potential future work are discussed in Section 4. Lastly, in Section 5, we conclude our present work.

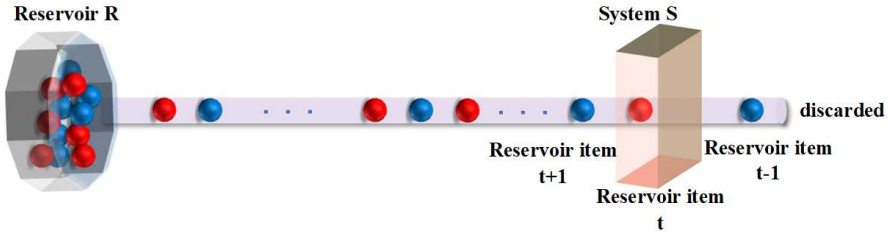

Figure 2. Framework of a quantum reservoir consisting of a sequence of qubits initialized at a different state in each pair.

2. Mathematical Model of the System Setup and Quantification of the Estimation Precision

In the system setting shown in Figure 2, quantum reservoir R is composed of a sequence of separable qubits that are alternately prepared at two different initial states. From a control-theory point of view, the initial states of qubits play the role of control variables, and the harmonic oscillator is considered the target system. In other words, our aim was to control the final state of the harmonic oscillator with the parameter to be estimated embedded, which could be used for quantum metrology. In this section, we recall the detailed mathematical description of this reservoir engineering system. A stabilized squeezed state with an associated QFI is also provided without taking into account photonic loss through the oscillator to the environment (the ideal case) [22–24].

Specifically, as shown in Figure 2, since the reservoir qubits were initialized at states $|\psi_{qred}\rangle$, $|\psi_{qblue}\rangle$, $|\psi_{qred}\rangle$, $|\psi_{qblue}\rangle$, $\cdots$, we could regard one pair of qubits as a whole. In particular, $|\psi_{qred}\rangle = \cos u_1 |g\rangle + \sin u_1 |e\rangle$ and $|\psi_{qblue}\rangle = \cos u_2 |g\rangle + \sin u_2 |e\rangle$, where the parameters $u_{1,2} \in [0, \frac{\pi}{4})$. According to the results in [23], we know that when the initial phases of the qubits are the same, it could benefit the precision; thus, the initial phases of the qubits were set to zero. Equivalently, the initial state for one pair of qubits can also be described by

$$\begin{aligned} |\psi_{q^2}(0)\rangle = &\cos u_1 \cos u_2 |gg\rangle + \sin u_1 \sin u_2 |ee\rangle \\ &+ \cos u_1 \sin u_2 |ge\rangle + \sin u_1 \cos u_2 |eg\rangle . \end{aligned} \tag{1}$$

Each qubit interacts with the harmonic oscillator for a short period of time t_r according to the following Jaynes–Cummings Hamiltonian:

$$\boldsymbol{H}_{JC} = i\frac{\Omega}{2}(|g\rangle\langle e|\boldsymbol{a}^{\dagger} - |e\rangle\langle g|\boldsymbol{a}), \tag{2}$$

where Ω the Rabi oscillation frequency, $\boldsymbol{a}$ is the oscillator mode's annihilation operator, and $|g\rangle and |e\rangle$ are the qubit's ground and excited states, respectively. The unitary propagator describing qubit–oscillator interaction is then

$$\boldsymbol{U}_r = |g\rangle\langle g| \cos\theta_{\boldsymbol{N}} + |e\rangle\langle e| \cos\theta_{\boldsymbol{N+I}} - |e\rangle\langle g|\boldsymbol{a}\frac{\sin\theta_{\boldsymbol{N}}}{\sqrt{\boldsymbol{N}}} + |g\rangle\langle e|\frac{\sin\theta_{\boldsymbol{N}}}{\sqrt{\boldsymbol{N}}}\boldsymbol{a}^{\dagger}, \tag{3}$$

where

$$\theta_N = \theta\sqrt{\boldsymbol{N}} = \tfrac{1}{2}\Omega t_r \sum_n \sqrt{n}|n\rangle\langle n|,$$

where $\boldsymbol{N} = \boldsymbol{a}^\dagger \boldsymbol{a}$ is the photon number operator, $|n\rangle (n = 0, 1, 2, ...)$ are the Fock states of the harmonic oscillator mode, and $\boldsymbol{I}$ is the identity operator. Qubit–oscillator interactions operate in the weakly coupled regime; thus, $\theta = \frac{1}{2}\Omega t_r$ (the effective qubit–oscillator coupling strength to be estimated) is sufficiently small.

We first briefly present the scenario where all qubits are initialized at the same state, i.e., $|\psi\rangle = \cos u\,|g\rangle + \sin u\,|e\rangle$ with $u \in [0, \frac{\pi}{4})$, as shown in Figure 1.

By assuming that θ is sufficiently small, the oscillator state can be stabilized at coherent state $|\alpha\rangle$ with $\alpha = \frac{\tan 2u}{\theta}$ (u is required to be sufficiently small in order to guarantee the stabilization). The corresponding convergence rate is $\kappa_c = \theta^2 \cos 2u$.

Without considering the dissipation to the environment, we now focus on the scenario where the reservoir qubits are initialized at states $|\psi_{qred}\rangle$, $|\psi_{qblue}\rangle$, $|\psi_{qred}\rangle$, $|\psi_{qblue}\rangle$, $\cdots$, as shown in Figure 2. Following a similar procedure to that in [23], the Lindblad master equation for oscillator state ρ by taking the continuous-time approximation is as follows:

$$\tfrac{d}{dt}\rho(t) = -i[\boldsymbol{H}, \rho(t)] + \sum_{j=1}^{3} \mathcal{L}(\boldsymbol{L}_j)\rho(t), \tag{4}$$

Superoperator $\mathcal{L}(\boldsymbol{L})$ denotes the Lindbladian that is defined by

$$\mathcal{L}(\boldsymbol{L})\rho(t) = \boldsymbol{L}\rho(t)\boldsymbol{L}^\dagger - \frac{1}{2}\rho(t)\boldsymbol{L}^\dagger\boldsymbol{L} - \frac{1}{2}\boldsymbol{L}^\dagger\boldsymbol{L}\rho(t),$$

with $\boldsymbol{L}$ being the coupling operator. The Hamiltonian and coupling operators in Equation (4) are given by

$$\begin{aligned}
&\boldsymbol{H} = -i\theta(\boldsymbol{Q} - \boldsymbol{Q}^\dagger),\ \boldsymbol{Q} = \cos(u_1 - u_2)\sin(u_1 + u_2)\boldsymbol{a},\\
&\boldsymbol{L_1} = \sqrt{2}\theta\cos u_1 \cos u_2 \boldsymbol{a} - \sqrt{2}\theta \sin u_1 \sin u_2 \boldsymbol{a}^\dagger,\\
&\boldsymbol{L_2} = \theta\sin(u_1 + u_2)\boldsymbol{a},\ \boldsymbol{L_3} = \theta\sin(u_1 + u_2)\boldsymbol{a}^\dagger.
\end{aligned}$$

In order to stabilize the oscillator state, we require

$$\sin(u_1 + u_2) \text{ is sufficiently small, and } \cos(u_1 + u_2) > 0,$$

such that $\boldsymbol{L_1}$ dominates the dynamics. Then, reservoir qubits can drive the oscillator to a squeezed state $|\alpha, r\rangle$ with the parameters

$$\alpha = \frac{\tan(u_1 + u_2)}{\theta}, \tag{5a}$$

$$r = \frac{1}{2}\ln\frac{\cos(u_1 - u_2)}{\cos(u_1 + u_2)}. \tag{5b}$$

In general, α can be complex for a squeezed state of the $|\alpha, r\rangle$ form. However, α in Equation (5a) is real by initially preparing the qubits at $|\psi_{qred}\rangle$, $|\psi_{qblue}\rangle$, $|\psi_{qred}\rangle$, $|\psi_{qblue}\rangle$, $\cdots$.

This can be proven by applying the displacement and squeezing transformation to $\rho(t)$ as follows:

$$\widetilde{\rho}(t) = \boldsymbol{S}^\dagger(r)\boldsymbol{D}^\dagger(\alpha)\rho(t)\boldsymbol{D}(\alpha)\boldsymbol{S}(r), \tag{6}$$

$$\widetilde{\boldsymbol{H}} = \boldsymbol{S}^\dagger(r)\boldsymbol{D}^\dagger(\alpha)\boldsymbol{H}\boldsymbol{D}(\alpha)\boldsymbol{S}(r), \tag{7}$$

$$\widetilde{\boldsymbol{L_1}} = \boldsymbol{S}^\dagger(r)\boldsymbol{D}^\dagger(\alpha)\boldsymbol{L_1}\boldsymbol{D}(\alpha)\boldsymbol{S}(r), \tag{8}$$

which results in the following.

$$\frac{\mathrm{d}\widetilde{\rho}(t)}{\mathrm{d}t} = \theta^2\left(\frac{\cos^3(u_1-u_2)}{2\cos(u_1+u_2)} + \frac{\cos^3(u_1+u_2)}{2\cos(u_1-u_2)} + \cos(u_1-u_2)(u_1+u_2)\right)\mathcal{L}(\boldsymbol{a})\widetilde{\rho}(t), \quad (9)$$

with α and r given in Equation (5). By defining the Lyapunov function:

$$V(t) = \mathrm{Tr}(\boldsymbol{a}^\dagger \boldsymbol{a}\boldsymbol{S}^\dagger(r)\boldsymbol{D}^\dagger(\alpha)\rho(t)\boldsymbol{D}(\alpha)\boldsymbol{S}(r)),$$

we can further obtain that

$$\tfrac{d}{dt}V(t) = \mathrm{Tr}(\boldsymbol{a}^\dagger \boldsymbol{a}\dot{\widetilde{\rho}}(t)) = -2\theta^2(\cos^2 u_1 \cos^2 u_2 - \sin^2 u_1 \sin^2 u_2)V(t) = -\kappa_s V(t), \quad (10)$$

Thus, κ_s denotes the convergence rate.

For a squeezed state $|\alpha, r\rangle$, one can calculate the QFI $\mathcal{F}_Q$ by using the following method (see, e.g., [29]),

$$\mathcal{F}_Q = 2\frac{\mathrm{d}\nu^\dagger}{\mathrm{d}\theta}\sigma^{-1}\frac{\mathrm{d}\nu}{\mathrm{d}\theta},$$

where

$$\nu = (\alpha, \alpha^*)^T, \quad \sigma = \begin{bmatrix} \cosh 2r & \sinh 2r \\ \sinh 2r & \cosh 2r \end{bmatrix}.$$

This formula can be derived on the basis of the definition of the QFI associated with the Bures distance between ρ_θ and $\rho_{\theta+\mathrm{d}\theta}$ as follows:

$$\mathrm{d}^2_{Bures}(\rho_\theta, \rho_{\theta+\mathrm{d}\theta}) = \frac{1}{4}\mathcal{F}_Q \mathrm{d}\theta^2.$$

In this stabilization scenario, we are dealing with the steady state; therefore, the time cost is supposed to be included to evaluate estimation in a control protocol [30]. The appropriate QFI for the steady state is, thus, given by

$$\mathcal{F}_s = \mathcal{F}_Q \kappa_s^2 \quad (11)$$

by incorporating the convergence rate. The QFI associated with the squeezed state $|\frac{\tan(u_1+u_2)}{\theta}, \frac{1}{2}\ln\frac{\cos(u_1-u_2)}{\cos(u_1+u_2)}\rangle$ is (subscript s stands for "squeezed state")

$$\mathcal{F}_s = \frac{16\sin^2(u_1+u_2)\cos^3(u_1-u_2)}{\cos(u_1+u_2)}. \quad (12)$$

3. Quantification of the Estimation Precision in the Presence of Photonic Loss to the Environment

In Section 2, we present the mathematical description of the system setup, and calculate QFI on the basis of the results in [23] without considering dissipation to the environment. However, in practice, it is inevitable that the qubit–oscillator quantum reservoir engineering system undergoes photonic loss to the environment during the whole process. Therefore, in this section, the associated QFI is amended due to the noisy dynamics of open quantum systems [22,31]. We included the energy decay of the harmonic oscillator via the annihilation operator in a zero-temperature bath. Over a short period of time t_r compared to the oscillator characteristic lifetime $1/\gamma$, the corresponding effect could be modeled with the Kraus map: $\rho \mapsto \boldsymbol{M}_0\rho\boldsymbol{M}_0^\dagger + \boldsymbol{M}_1\rho\boldsymbol{M}_1^\dagger$, where the propagators

$$\boldsymbol{M}_0 = \boldsymbol{I} - \frac{\gamma t_r}{2}\boldsymbol{a}^\dagger\boldsymbol{a}, \ \boldsymbol{M}_1 = \sqrt{\gamma t_r}\boldsymbol{a}. \quad (13)$$

3.1. Convergence towards a Coherent State

We first consider the scenario where each qubit is prepared at the same state that interacts with the harmonic oscillator, as shown in Figure 1, taking into account the energy decay from the oscillator to the environment. The following Kraus map could then be used to describe the evolution of the oscillator state:

$$\begin{aligned}\rho(t+1) =& \boldsymbol{M}_0(\boldsymbol{M}_g\rho(t)\boldsymbol{M}_g^\dagger + \boldsymbol{M}_e\rho(t)\boldsymbol{M}_e^\dagger)\boldsymbol{M}_0^\dagger \\ &+ \boldsymbol{M}_1(\boldsymbol{M}_g\rho(t)\boldsymbol{M}_g^\dagger + \boldsymbol{M}_e\rho(t)\boldsymbol{M}_e^\dagger)\boldsymbol{M}_1^\dagger.\end{aligned} \tag{14}$$

Assuming that $\theta \ll 1$ and $\gamma t_r \ll 1$, we expanded the Kraus map given in Equation (14) to the second order in θ and the first order in γt_r, and the following approximated Lindblad master equation could be obtained:

$$\begin{aligned}\frac{\mathrm{d}\rho(t)}{\mathrm{d}t} =& \theta^2\cos^2 u\mathcal{L}(\boldsymbol{a})\rho(t) + \theta^2\sin^2 u\mathcal{L}(\boldsymbol{a}^\dagger)\rho(t) + \theta\cos u\sin u[\rho(t), \boldsymbol{a}-\boldsymbol{a}^\dagger] \\ &- \frac{\gamma t_r}{2}\boldsymbol{a}^\dagger\boldsymbol{a}\rho(t) - \frac{\gamma t_r}{2}\rho(t)\boldsymbol{a}^\dagger\boldsymbol{a} + \gamma t_r\boldsymbol{a}\rho(t)\boldsymbol{a}^\dagger.\end{aligned} \tag{15}$$

By imposing the displacement transformation onto $\rho(t)$, we could obtain the corresponding Lindblad master equation for the transformed $\widetilde{\rho}(t)$:

$$\begin{aligned}\frac{\mathrm{d}\widetilde{\rho}(t)}{\mathrm{d}t} =& (\theta^2\cos^2 u + \gamma t_r)\mathcal{L}(\boldsymbol{a})\widetilde{\rho}(t) + \theta^2\sin^2 u\mathcal{L}(\boldsymbol{a}^\dagger)\widetilde{\rho}(t) \\ &+ (\frac{1}{2}\theta^2\cos^2 u\alpha - \theta\sin u\cos u - \frac{1}{2}\theta^2\sin^2 u\alpha + \frac{\alpha\gamma t_r}{2})[\widetilde{\rho}(t), \boldsymbol{a}^\dagger] \\ &+ (\frac{1}{2}\theta^2\sin^2 u\alpha^* + \theta\sin u\cos u - \frac{1}{2}\theta^2\cos^2 u\alpha^* - \frac{\alpha^*\gamma t_r}{2})[\widetilde{\rho}(t), \boldsymbol{a}].\end{aligned} \tag{16}$$

On the basis of the equation of motion above, the coherent state $|\alpha\rangle$ with $\alpha = \frac{\theta\sin 2u}{\theta^2\cos 2u+\gamma t_r}$ of the oscillator could be stabilized, provided that $\sin u$ was sufficiently small (e.g. $\sin u \ll 1$). Convergence was guaranteed by the $\theta^2\cos 2u + \gamma t_r \geq 0$ condition, which could be obtained by considering Lyapunov equation $V(t) = \mathrm{Tr}(\boldsymbol{a}^\dagger\boldsymbol{a}\boldsymbol{D}^\dagger(\alpha)\rho(t)\boldsymbol{D}(\alpha))$ and its derivative

$$\begin{aligned}\tfrac{d}{dt}V(t) &= 2(\theta^2\sin^2 u - \theta^2\cos^2 u - \gamma t_r)\,\mathrm{Tr}(\widetilde{\rho}(t)a^\dagger a) \\ &= -2(\theta^2\cos 2u + \gamma t_r)V(t) = -\kappa_{dc}V(t).\end{aligned} \tag{17}$$

In order to realize $\frac{d}{dt}V(t) \leq 0$, $\kappa_{dc} = 2\left(\theta^2\cos 2u + \gamma t_r\right) \geq 0$ is required, with κ_{dc} as the convergence rate.

In a similar way, to calculate the QFI, as presented in Section 2, we could obtain the QFI regarding a coherent state when dissipation to the environment is taken into account as follows (subscripts d and c stand for "dissipation" and "coherent", respectively):

$$\mathcal{F}_{dc} = \frac{16\sin^2 2u(\gamma t_r - \theta^2\cos 2u)^2}{(\theta^2\cos 2u + \gamma t_r)^2}. \tag{18}$$

3.2. Convergence towards a Squeezed State

In this part, we focus on the scenario where the reservoir qubits are initialized at the states $|\psi_{qred}\rangle, |\psi_{qblue}\rangle, |\psi_{qred}\rangle, |\psi_{qblue}\rangle, \cdots$, as shown in Figure 2. These qubits interact with the harmonic oscillator in the presence of oscillator's phton loss to the environment. The evolution of the oscillator state after it interacted with one pair of qubits can be described with the following Kraus map:

$$\begin{aligned}\rho(t+1) =& \boldsymbol{M}_0\boldsymbol{M}_0(\boldsymbol{M}_{gg}\rho(t)\boldsymbol{M}_{gg}^\dagger + \boldsymbol{M}_{ge}\rho(t)\boldsymbol{M}_{ge}^\dagger + \boldsymbol{M}_{eg}\rho(t)\boldsymbol{M}_{eg}^\dagger + \boldsymbol{M}_{ee}\rho(t)\boldsymbol{M}_{ee}^\dagger)\boldsymbol{M}_0^\dagger\boldsymbol{M}_0^\dagger \\ &+\boldsymbol{M}_0\boldsymbol{M}_1(\boldsymbol{M}_{gg}\rho(t)\boldsymbol{M}_{gg}^\dagger + \boldsymbol{M}_{ge}\rho(t)\boldsymbol{M}_{ge}^\dagger + \boldsymbol{M}_{eg}\rho(t)\boldsymbol{M}_{eg}^\dagger + \boldsymbol{M}_{ee}\rho(t)\boldsymbol{M}_{ee}^\dagger)\boldsymbol{M}_1^\dagger\boldsymbol{M}_0^\dagger\end{aligned}$$

$$+\boldsymbol{M}_1\boldsymbol{M}_0(\boldsymbol{M}_{gg}\rho(t)\boldsymbol{M}_{gg}^\dagger+\boldsymbol{M}_{ge}\rho(t)\boldsymbol{M}_{ge}^\dagger+\boldsymbol{M}_{eg}\rho(t)\boldsymbol{M}_{eg}^\dagger+\boldsymbol{M}_{ee}\rho(t)\boldsymbol{M}_{ee}^\dagger)\boldsymbol{M}_0^\dagger\boldsymbol{M}_1^\dagger$$
$$+\boldsymbol{M}_1\boldsymbol{M}_1(\boldsymbol{M}_{gg}\rho(t)\boldsymbol{M}_{gg}^\dagger+\boldsymbol{M}_{ge}\rho(t)\boldsymbol{M}_{ge}^\dagger+\boldsymbol{M}_{eg}\rho(t)\boldsymbol{M}_{eg}^\dagger+\boldsymbol{M}_{ee}\rho(t)\boldsymbol{M}_{ee}^\dagger)\boldsymbol{M}_1^\dagger\boldsymbol{M}_1^\dagger.$$

where the propagators

$$\begin{aligned}
\boldsymbol{M}_{gg} =& \cos u_1\cos u_2\cos^2\theta_{\boldsymbol{N}}+\cos u_1\sin u_2\cos\theta_{\boldsymbol{N}}\frac{\sin\theta_{\boldsymbol{N}}}{\sqrt{\boldsymbol{N}}}\boldsymbol{a}^\dagger\\
&+\sin u_1\cos u_2\frac{\sin\theta_{\boldsymbol{N}}}{\sqrt{\boldsymbol{N}}}\boldsymbol{a}^\dagger\cos\theta_{\boldsymbol{N}}+\sin u_1\sin u_2\frac{\sin\theta_{\boldsymbol{N}}}{\sqrt{\boldsymbol{N}}}\boldsymbol{a}^\dagger\frac{\sin\theta_{\boldsymbol{N}}}{\sqrt{\boldsymbol{N}}}\boldsymbol{a}^\dagger,\\
\boldsymbol{M}_{ge} =& -\cos u_1\cos u_2\cos\theta_{\boldsymbol{N}}\boldsymbol{a}\frac{\sin\theta_{\boldsymbol{N}}}{\sqrt{\boldsymbol{N}}}+\cos u_1\sin u_2\cos\theta_{\boldsymbol{N}}\cos\theta_{\boldsymbol{N+I}}\\
&-\sin u_1\cos u_2\sin^2\theta_{\boldsymbol{N}}+\sin u_1\sin u_2\frac{\sin\theta_{\boldsymbol{N}}}{\sqrt{\boldsymbol{N}}}\boldsymbol{a}^\dagger\cos\theta_{\boldsymbol{N+I}},\\
\boldsymbol{M}_{eg} =& -\cos u_1\cos u_2\boldsymbol{a}\frac{\sin\theta_{\boldsymbol{N}}}{\sqrt{\boldsymbol{N}}}\cos\theta_{\boldsymbol{N}}-\cos u_1\sin u_2\sin^2\theta_{\boldsymbol{N+I}}\\
&+\sin u_1\cos u_2\cos\theta_{\boldsymbol{N+I}}\cos\theta_{\boldsymbol{N}}+\sin u_1\sin u_2\cos\theta_{\boldsymbol{N+I}}\frac{\sin\theta_{\boldsymbol{N}}}{\sqrt{\boldsymbol{N}}}\boldsymbol{a}^\dagger,\\
\boldsymbol{M}_{ee} =& \cos u_1\cos u_2\boldsymbol{a}\frac{\sin\theta_{\boldsymbol{N}}}{\sqrt{\boldsymbol{N}}}\boldsymbol{a}\frac{\sin\theta_{\boldsymbol{N}}}{\sqrt{\boldsymbol{N}}}-\cos u_1\sin u_2\boldsymbol{a}\frac{\sin\theta_{\boldsymbol{N}}}{\sqrt{\boldsymbol{N}}}\cos\theta_{\boldsymbol{N+I}}\\
&-\sin u_1\cos u_2\cos\theta_{\boldsymbol{N+I}}\boldsymbol{a}\frac{\sin\theta_{\boldsymbol{N}}}{\sqrt{\boldsymbol{N}}}+\sin u_1\sin u_2\cos^2\theta_{\boldsymbol{N+I}}.
\end{aligned}$$

In this scenario, we required the number of qubits to be even. Assuming that $\theta \ll 1$ and $\gamma t_r \ll 1$ (in practice, γt_r is supposed to be of the $o(\theta^3)$ order), we expanded this Kraus map to the second order in θ, and first order in γt_r; then, the Kraus map can be approximated with the following Lindblad master equation:

$$\begin{aligned}
\frac{\mathrm{d}\rho(t)}{\mathrm{d}t} =& -i[\boldsymbol{H},\rho(t)]+\sum_{j=1}^{3}\mathcal{L}(\boldsymbol{L}_j)\rho(t)\\
&+2\gamma t_r\mathcal{L}(\boldsymbol{a})(\boldsymbol{M}_{gg}\rho(t)\boldsymbol{M}_{gg}^\dagger+\boldsymbol{M}_{ge}\rho(t)\boldsymbol{M}_{ge}^\dagger\\
&+\boldsymbol{M}_{eg}\rho(t)\boldsymbol{M}_{eg}^\dagger+\boldsymbol{M}_{ee}\rho(t)\boldsymbol{M}_{ee}^\dagger).
\end{aligned}\tag{19}$$

Equation (19) stabilizes a squeezed state $|\alpha, r\rangle$ with

$$\alpha=\frac{\tan(u_1+u_2)}{\theta+\gamma t_r},\tag{20a}$$
$$r=\frac{1}{4}\ln\frac{\theta^2\cos^2(u_1-u_2)+\gamma t_r}{\theta^2\cos^2(u_1+u_2)+\gamma t_r},\tag{20b}$$

Provided that $\sin(u_1+u_2)$ is sufficiently small. This can be proven by applying the displacement and squeezing transformations to transform the original density operator $\rho(t)$ into $\widetilde{\rho}(t)$ as follows:

$$\widetilde{\rho}(t)=\boldsymbol{S}^\dagger(r)\boldsymbol{D}^\dagger(\alpha)\rho(t)\boldsymbol{D}(\alpha)\boldsymbol{S}(r),$$

whose evolution can be described by

$$\begin{aligned}
\frac{\mathrm{d}\widetilde{\rho}(t)}{\mathrm{d}t} =& [2\theta^2(\cos u_1\cos u_2\cosh r+\sin u_1\sin u_2\sinh r)^2+2\gamma t_r\cosh^2 r]\boldsymbol{\mathcal{L}}(\boldsymbol{a})\widetilde{\rho}(t)\\
&+[2\theta^2(\cos u_1\cos u_2\cosh r+\sin u_1\sin u_2\sinh r)^2+2\gamma t_r\sinh^2 r]\boldsymbol{\mathcal{L}}(\boldsymbol{a}^\dagger)\widetilde{\rho}(t)\\
&+\theta l(\sinh r+\cosh r)[\boldsymbol{a}^\dagger,\widetilde{\rho}(t)]+\theta l(\sinh r+\cosh r)[\widetilde{\rho}(t),\boldsymbol{a}]\\
&+\theta^2(\cos u_1\cos u_2\alpha-\sin u_1\sin u_2\alpha^*)
\end{aligned}$$

$$
\begin{aligned}
&\times(\cos u_1\cos u_2\cosh r+\sin u_1\sin u_2\sinh r)[\widetilde{\rho}(t),\boldsymbol{a}^{\dagger}]\\
&+\theta^2(\sin u_1\sin u_2\alpha-\cos u_1\cos u_2\alpha^*)\\
&\times(\cos u_1\cos u_2\sinh r+\sin u_1\sin u_2\cosh r)[\boldsymbol{a}^{\dagger},\widetilde{\rho}(t)]\\
&+\theta^2(\cos u_1\cos u_2\alpha^*-\sin u_1\sin u_2\alpha)\\
&\times(\cos u_1\cos u_2\cosh r+\sin u_1\sin u_2\sinh r)[\boldsymbol{a},\widetilde{\rho}(t)]\\
&+\theta^2(\sin u_1\sin u_2\alpha^*-\cos u_1\cos u_2\alpha)\\
&\times(\cos u_1\cos u_2\sinh r+\sin u_1\sin u_2\cosh r)[\widetilde{\rho}(t),\boldsymbol{a}]\\
&+\gamma t_r(\sinh r\alpha^*+\cosh r\alpha)[\widetilde{\rho}(t),\boldsymbol{a}^{\dagger}]-\gamma t_r(\sinh r\alpha+\cosh r\alpha^*)[\widetilde{\rho}(t),\boldsymbol{a}]\\
&+\theta^2(\cos u_1\cos u_2\cosh r+\sin u_1\sin u_2\sinh r)\\
&\times(\cos u_1\cos u_2\sinh r+\sin u_1\sin u_2\cosh r)([[\widetilde{\rho}(t),\boldsymbol{a}^{\dagger}],\boldsymbol{a}]+[[\widetilde{\rho}(t),\boldsymbol{a}],\boldsymbol{a}])\\
&+\gamma t_r\sinh r\cosh r([[\widetilde{\rho}(t),\boldsymbol{a}^{\dagger}],\boldsymbol{a}]+[[\widetilde{\rho}(t),\boldsymbol{a}],\boldsymbol{a}]).
\end{aligned}
\tag{21}
$$

Therefore, if we chose $4r=\ln\frac{\theta^2\cos^2(u_1-u_2)+\gamma t_r}{\theta^2\cos^2(u_1+u_2)+\gamma t_r}$ and $\alpha=\frac{\tan(u_1+u_2)}{\theta+\gamma t_r}$, Equation (22) could be equivalently written as follows:

$$
\frac{\mathrm{d}\widetilde{\rho}(t)}{\mathrm{d}t}=\epsilon_{ds}\mathcal{L}(\boldsymbol{a})\widetilde{\rho}(t),
\tag{22}
$$

where

$$
\begin{aligned}
\epsilon_{ds}=&\frac{1}{2}(\theta^2cos^2(u_1-u_2)+\gamma t_r)\sqrt{\frac{\theta^2\cos^2(u_1-u_2)+\gamma t_r}{\theta^2\cos^2(u_1+u_2)+\gamma t_r}}\\
&+\frac{1}{2}(\theta^2cos^2(u_1+u_2)+\gamma t_r)\sqrt{\frac{\theta^2\cos^2(u_1+u_2)+\gamma t_r}{\theta^2\cos^2(u_1-u_2)+\gamma t_r}}\\
&+\theta^2\cos(u_1-u_2)\cos(u_1+u_2)+\gamma t_r.
\end{aligned}
$$

Convergence towards a squeezed state of the oscillator in such a scenario also requires $(1-2\gamma t_r)\cos(u_1-u_2)\cos(u_1+u_2)\geq 0$. This can be viewed by taking into consideration Lyapunov equation $V(t)=\mathrm{Tr}(\boldsymbol{a}^{\dagger}\boldsymbol{a}\boldsymbol{S}^{\dagger}(r)\boldsymbol{D}^{\dagger}(\alpha)\rho(t)\boldsymbol{D}(\alpha)\boldsymbol{S}(r))$. Then, it is not difficult to find that

$$
\tfrac{d}{dt}V(t)=-2\theta^2(1-2\gamma t_r)\cos(u_1-u_2)\cos(u_1+u_2)V(t)=-\kappa_{ds}V(t),
\tag{23}
$$

which should make $\frac{d}{dt}V(t)\leq 0$ hold; thus, $\kappa_{ds}=2\theta^2(1-2\gamma t_r)\cos(u_1-u_2)\cos(u_1+u_2)$ is the corresponding convergence rate.

In a similar way, to calculate the QFI as presented in Section 2, we could obtain the QFI regarding a squeezed state when photonic loss from the oscillator to the environment is taken into account as follows (subscripts d and s stand for "dissipation" and "squeezed", respectively):

$$
\begin{aligned}
\mathcal{F}_{ds}=&4\kappa_{ds}^2|\frac{d\alpha}{d\theta}|^2(\cosh 2r+\sinh 2r),\\
=&16\theta^4\frac{\sin^2 u_s}{(\theta+\gamma t_r)^4}\sqrt{\frac{\theta^2\cos^2 u_d+\gamma t_r}{\theta^2\cos^2 u_s+\gamma t_r}}(1-2\gamma t_r)^2\cos^2 u_d,
\end{aligned}
\tag{24}
$$

where $u_d=u_1-u_2$ and $u_s=u_1+u_2$. Apparently, the QFI $\mathcal{F}_{ds}$ given in Equation (24) could degenerate into the QFI $\mathcal{F}_s$ given in Equation (12) when $\gamma=0$. This, in turn, verified the consistency and correctness of our derivation.

3.3. Analysis of Enhanced Estimation Precision via the Time-Varying Reservoir

In this subsection, we show the significant increase in QFI in the presence of photonic loss from the oscillator to the environment while the oscillator is converging into a squeezed state instead of a coherent state.

Referring to the physical parameters in [22], we set dissipation rate $\gamma = 20\,\text{Hz}$, and the interaction time t_r to 1.25×10^{-2} ms, with the coupling strength mostly chosen to be $\theta = \frac{\pi}{8}$ in simulations. For example, if u was set to $u = 0.1$ when all the reservoir qubits were initialized at the same state $|\psi\rangle = \cos 0.1\,|g\rangle + \sin 0.1\,|e\rangle$, the final state of the oscillator could be visualized through the Wigner distribution as depicted in Figure 3a. The state in this case was coherent.

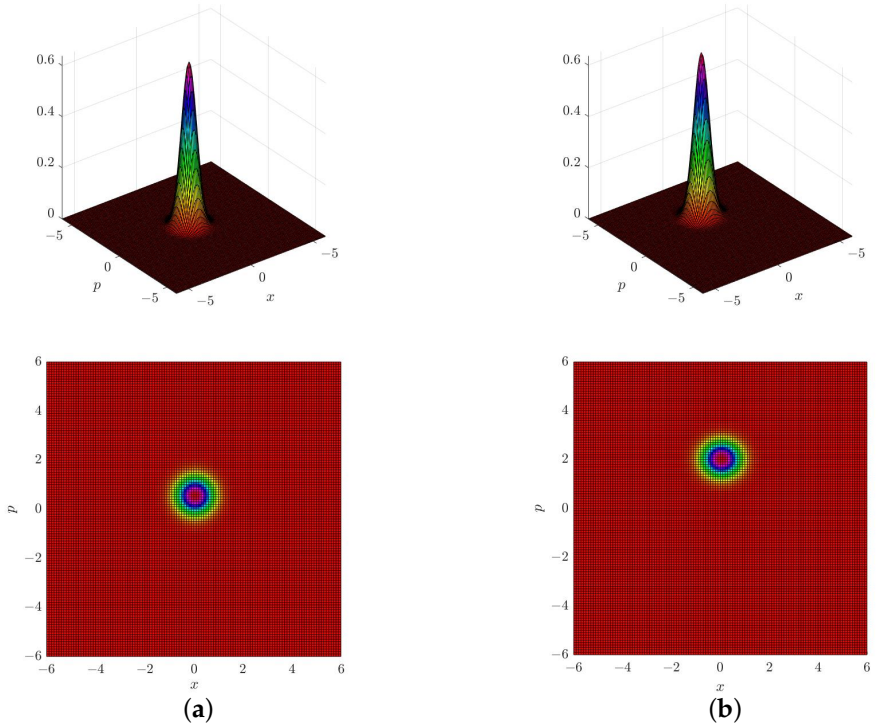

Figure 3. Wigner distribution for the steady state of the harmonic oscillator in the presence of photonic loss with dissipation rate $\gamma = 20\,\text{Hz}$ and coupling strength $\theta = \frac{\pi}{8}$. (**a**) Wigner distribution for the coherent state at which the oscillator is stabilized when all reservoir qubits are prepared at the same state $|\psi\rangle = \cos 0.1\,|g\rangle + \sin 0.1\,|e\rangle$. (**b**) Wigner distribution for the squeezed state at which the oscillator is stabilized when reservoir qubits are prepared at states $|\psi_{qred}\rangle = \cos 0.395\,|g\rangle + \sin 0.395\,|e\rangle$, $|\psi_{qblue}\rangle = \cos 0.39\,|g\rangle + \sin 0.39\,|e\rangle, \cdots$.

By contrast, we chose $u_1 = 0.395$ and $u_2 = 0.39$, as shown in Figure 3b. Namely, the reservoir qubits were initially prepared at states $|\psi_{qred}\rangle = \cos 0.395\,|g\rangle + \sin 0.395\,|e\rangle$ and $|\psi_{qblue}\rangle = \cos 0.39\,|g\rangle + \sin 0.39\,|e\rangle$ pair by pair. Specifically, the Wigner distribution and the corresponding x–p phase for the final state of the oscillator are shown in Figure 3b, which shows that the state was squeezed. The Wigner distributions depicted in Figure 3 indicate that the form of steady states numerically obtained with the discrete-time Kraus map was consistent with the form of steady states theoretically derived on the basis of the approximated continuous-time Lindblad master equation.

In Figure 4, we plotted the values of QFI, as the initial states of qubits varied. For example, the blue dotted line in Figure 4b corresponds to the scenario where the oscillator was moving towards a coherent state in our simulation in the presence of photonic loss, with dissipation rate $\gamma = 20$ Hz. It is obvious that $\mathcal{F}_{dc} \leq 5.1$.

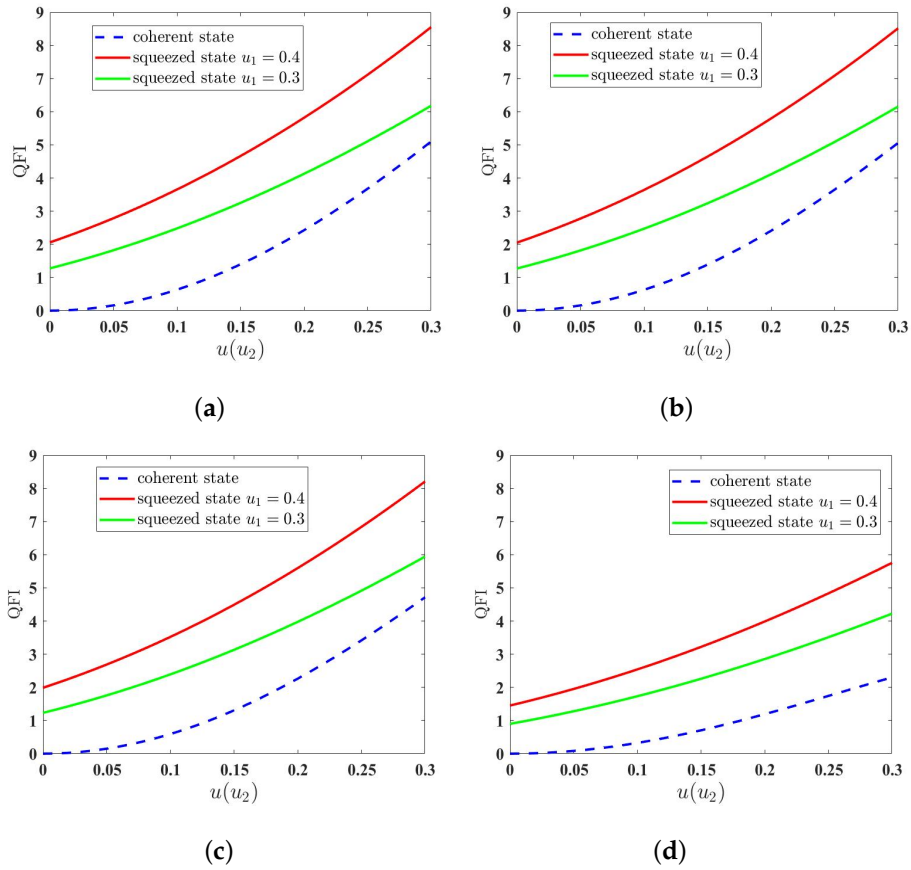

Figure 4. The values of QFI as the initial states of qubits vary when the harmonic oscillator is steered towards a coherent (blue dotted line) or squeezed (green and red solid lines) state in the presence of photonic loss, with interaction time $t_r = 1.25 \times 10^{-2}$ ms and Rabi frequency $\Omega = 20\pi$ KHz. More concretely, the red line corresponds to the case where the reservoir qubits were initialized in pairs with $u_1 = 0.4$, as u_2 varied from 0 to 0.3, while the green line corresponds to the case where the reservoir qubits were initialized in pairs with $u_1 = 0.3$, as u_2 varied from 0 to 0.3. By contrast, the blue dotted line corresponds to the case where the oscillator was moving towards a coherent state as u varied from 0 to 0.3, with dissipation rate (**a**) $\gamma = 0$ Hz, (**b**) $\gamma = 20$ Hz, (**c**) $\gamma = 200$ Hz, and (**d**) $\gamma = 2$ KHz.

In fact, according to Equation (18), the maximal $\mathcal{F}_{dc}$ could be obtained theoretically. By calculating the derivative of $\mathcal{F}_{dc}$ with respect to $\cos 2u$ ($u \in (0, u_{\max})$, $u_{max} < \frac{\pi}{4}$), we have that

$$\frac{\partial \mathcal{F}_{dc}}{\partial(\cos 2u)} = -32\frac{(\frac{\gamma t_r}{\theta^2} - \cos 2u)[2\frac{\gamma t_r}{\theta^2}(1 - \cos 2u^2) + \cos 2u(\frac{\gamma^2 t_r^2}{\theta^4} - \cos^2 2u)]}{(\frac{\gamma t_r}{\theta^2} + \cos 2u)^3}.$$

The stability condition also requires u to be sufficiently small. According to both numerical and theoretical analyses, $u_{max} \approx \frac{\pi}{10}$. Then, due to $\frac{\gamma t_r}{\theta^2} \ll 1$ and $0 < \frac{\gamma t_r}{\theta^2} < \frac{\cos^2 2u - 1 + \sqrt{2\cos^4 2u - 2\cos^2 2u + 1}}{\cos 2u}$, we have $\frac{\partial \mathcal{F}_{dc}}{\partial(\cos 2u)} < 0$ in this region, which indicates that $\mathcal{F}_{dc}$ increased when u increased ($\cos 2u$ decreased). Therefore, $\max(\mathcal{F}_{dc}) \approx 16(1 - \cos^2(2 \times \frac{\pi}{10})) = 5.53$.

The maximal $\mathcal{F}_{ds}$ can be obtained in a similar way. By calculating the derivative of $\mathcal{F}_{ds}$ with respect to u_s, i.e.,

$$\frac{\partial \mathcal{F}_{ds}}{\partial u_s} = 16\frac{\theta^4 \cos^2 u_d}{(\theta+\gamma t_r)^4}(1-2\gamma t_r)^2\left[2\sin u_s \cos u_s \sqrt{\frac{\theta^2\cos^2 u_d+\gamma t_r}{\theta^2\cos^2 u_s+\gamma t_r}} + \frac{\sin^2 u_s}{2\sqrt{\frac{\theta^2\cos^2 u_d+\gamma t_r}{\theta^2\cos^2 u_s+\gamma t_r}}}\frac{\theta^2\cos^2 u_d+\gamma t_r}{(\theta^2\cos^2 u_s+\gamma t_r)^2}\right],$$

For $\frac{\gamma t_r}{\theta^2} \ll 1$ and $u_s \in (0, \frac{\pi}{4}]$, $\frac{\partial \mathcal{F}_{ds}}{\partial u_s} > 0$ thus holds in this region. Additionally, u_d should be reduced in order to gain a larger value for $\mathcal{F}_{ds}$. Hence, for $u_s \in (0, u_{s_{max}}]$ ($u_{s_{max}}$ was around $\frac{\pi}{4}$ on the basis of our numerical and theoretical analysis), we have that $\max \mathcal{F}_{dc} \approx 16\sin^2(\frac{\pi}{4})/\cos(\frac{\pi}{4}) = 11.31$.

In contrast to the blue dotted line in Figure 4b, the red and green solid lines show the values of QFI concerning the steady state of the oscillator when the oscillator was stabilized at a squeezed state. Specifically, the red line corresponds to the case where the reservoir qubits were initialized in pairs with $u_1 = 0.4$, as u_2 varied from 0 to 0.3, while the green line corresponds to the case where the reservoir qubits were initialized in pairs with $u_1 = 0.3$, as u_2 varied from 0 to 0.3. In both cases, larger values of QFI were obtained compared to the case where all the qubits had been initialized at the same state (u varied from 0 to 0.3). Therefore, steering the oscillator towards a squeezed state enabled us to obtain a much larger value of QFI. If we chose $u_1 = 0.395$, and $u_2 = 0.39$, then $\mathcal{F}_{ds} = 11.25$ was almost double $\max \mathcal{F}_{dc}$. In addition, the red line presents larger values of QFI than the green line does. This is consistent with the theoretical analysis above that QFI increased as u_s increased when the oscillator was converging towards a squeezed state.

We also took into account the cases of $\gamma = 200$ Hz and $\gamma = 2$ KHz for comparison, with $\gamma = 0$ Hz included in Figure 4 in order to see the effect of dissipation. In particular, the cases of $\gamma = 0$ Hz, $\gamma = 200$ Hz and $\gamma = 2$ KHz are demonstrated in Figure 4a,c,d, respectively. Apparently, when γ grew, the value of QFI was reduced. It is not surprising that the values of QFI were almost the same for the two cases of $\gamma = 20$ Hz and $\gamma = 0$ Hz because, in principle, the steady state of the harmonic oscillator in the presence of photonic loss was not very different from the steady state in the ideal case when γ was sufficiently small.

On the other hand, it is also very important to estimate the resources that we must utilize. First, the convergence rates for the oscillator in the cases of stabilization at a coherent state and a squeezed state were theoretically compared as follows. Bearing in mind the assumption that $\frac{\gamma t_r}{\theta^2} \ll 1$, one has that

$$\begin{aligned}\frac{\kappa_{ds}}{\kappa_{dc}} &= \frac{(1-2\gamma t_r)\cos(u_1-u_2)\cos(u_1+u_2)}{\cos 2u + \frac{\gamma t_r}{\theta^2}} \\ &= \frac{(1-2\gamma t_r)\cos(u_1-u_2)\cos(u_1+u_2)}{2\cos^2 u - \left(1-\frac{\gamma t_r}{\theta^2}\right)} \\ &\approx \frac{\cos^2 u_1 + \cos^2 u_2 - 1}{2\cos^2 u - 1}.\end{aligned} \tag{25}$$

Therefore, the convergence rates in these two cases are typically of the same speed order. For example, if we chose $u_1 < u < \frac{\pi}{4}$ and $u_2 < u < \frac{\pi}{4}$, κ_{ds} was rendered to be larger than κ_{dc}, which indicates that fewer reservoir qubits were needed to harvest a squeezed state of the oscillator under such circumstances.

In Figure 5, we demonstrate the number of consumed reservoir qubits to reach the steady state of the oscillator. Here, $2n$ equals the number of qubits, and fidelity represents

the similarity between the current and steady states of the oscillator. Fidelity F can be calculated as follows [32]:

$$\mathrm{F}(\rho(t),\rho(\infty)) = \mathrm{Tr}(\sqrt{\sqrt{\rho(t)}\rho(\infty)\sqrt{\rho(t)}}). \tag{26}$$

In more concrete terms, as shown in Figure 5a, with $u_1 = 0.18$ and $u_2 = 0.12$, for $\theta = \frac{\pi}{12}$, $\theta = \frac{\pi}{10}$, and $\theta = \frac{\pi}{8}$, we plot how fidelity $\mathrm{F_s}$ varied as the number of qubits increased when the oscillator was converging towards a squeezed state using the red solid, blue dashed, and green dotted lines respectively. Additionally, Figure 5b shows, with $u = 0.2$, the evolution of $\mathrm{F_c}$ when the oscillator was converging towards a coherent state, where the red solid, blue dashed, and green dotted lines correspond to the cases where $\theta = \frac{\pi}{12}$, $\theta = \frac{\pi}{10}$ and $\theta = \frac{\pi}{8}$, respectively. Typically, fewer than 120 qubits (60 pairs of qubits) were needed to reach the steady state. The smaller the θ was, the more reservoir qubits were required to obtain the steady state, which could give increase estimation precision.

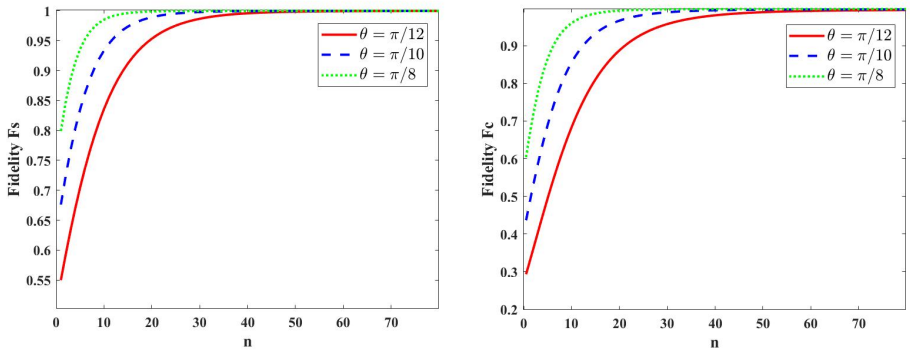

(**a**) (**b**)

Figure 5. Convergence towards a steady state of the oscillator with respect to different values of θ. Specifically, the red solid, blue dashed, and green dotted lines correspond to the case where the oscillator was (**a**) converging towards a squeezed state and (**b**) converging towards a coherent state with $\theta = \frac{\pi}{12}$, $\theta = \frac{\pi}{10}$ and $\theta = \frac{\pi}{8}$ respectively.

In our system setup, the oscillator could be stabilized at a squeezed state using the "time-varying" reservoir as specified in Section 3. Since the final state was not temporarily generated, it was easier and more convenient for us to impose or repeat the measurement of such a steady squeezed state in practice.

4. Discussion

In Section 3, we allowed dissipation through the oscillator to the environment. Our theoretical analysis shows that the steady state of the harmonic oscillator in the presence of photonic loss should not be very different from the steady state in the ideal case under the assumption of $\frac{\gamma t_r}{\theta^2} \ll 1$. This could also be observed by comparing the simulation results in Figure 4a,b. From another point of view, our system setup that could stabilize the oscillator state presented robustness to photonic loss.

On the other hand, the initial states of the reservoir qubits were chosen depending on the problems that needed explaining in our numerical simulation. In Figure 4, we focus on the comparative analysis regarding the values of QFI between different cases where the oscillator was steered towards a coherent or squeezed state. Therefore, u_2 varies from 0 to 0.3 in Figure 4 because u had to take values from 0 to 0.3 to ensure the convergence of the oscillator state. Squeezed states led to larger values of QFI when u_2 and u varied in the same range. In Figure 3b, a steady squeezed state of the oscillator is depicted. Parameters $u_1 = 0.395$ and $u_2 = 0.39$ were, thus, chosen in this case in order to render the squeezing

obvious according to Equation (20). In Figure 5, we chose $u_1 = 0.18$ and $u_2 = 0.12$ ($u = 0.2$) since the purpose was to show that, by appropriately preparing the initial states of qubits (i.e. $u_1 < u = 0.2 < \frac{\pi}{4}$ and $u_2 < u = 0.2 < \frac{\pi}{4}$), convergence rate κ_{ds} when the oscillator was steered towards a squeezed state could be made larger than convergence rate κ_{dc} when the oscillator was steered towards a coherent state according to Equation (26). There was, indeed, a trade-off between fast convergence and strong squeezing strength (large value of QFI).

In the future, we will consider variants in the system setup by adjusting the initial states of reservoir qubits, and the interaction between each qubit and the oscillator with the purpose of seeking other applications in quantum computation and quantum metrology. In terms of other imperfections in practice, dephasing and relaxation errors playing the role of noise to the preparation of qubits states, along with missing qubits, may also be considered.

5. Conclusions

Mainly inspired by [20] where the Serge Haroche experimental setting was utilized to restore the Heisenberg limit regarding estimating the coupling strength between each qubit and the harmonic oscillator, in this paper, we altered the setting by incorporating a time-varying quantum reservoir that enabled us to obtain even higher estimation precision. The contributions of this paper are threefold. First, in contrast to the results in [23], we took into account photonic loss through the harmonic oscillator to the environment and analytically provided the steady state of the oscillator under such circumstances. With consecutive pairs of separable time-varying input qubits, we could stabilize the oscillator at a squeezed state. The corresponding convergence condition and convergence rate were given as well. Second, we proved that stabilizing the oscillator at a squeezed state could improve the estimation precision of qubit–oscillator coupling strength by theoretically calculating the QFI, which was demonstrated in and verified by simulation examples in comparison with the case where all the qubits were prepared at an identical state, as discussed in the previous work. Last but not least, we discuss the approximate number of reservoir qubits that needs to be utilized for the oscillator to reach the final state. By appropriately choosing the initial qubit states, the time-varying reservoir could help us in achieving faster convergence. Since this final state of the oscillator could stay steady by absorbing qubits from the reservoir, it is more convenient for implementing quantum metrology experimentally.

Author Contributions: Conceptualization, Z.M.; methodology, Y.X. and Z.M.; formal analysis, Y.X., W.G. and Z.M.; data curation, Y.X., W.G. and Z.M.; writing—original draft preparation, Y.X. and Z.M.; writing—review and editing, Z.M.; visualization, Y.X.; supervision, Z.M.; project administration, Z.M..; funding acquisition, Z.M. All authors have read and agreed to the published version of the manuscript.

Funding: This research was funded by National Natural Science Foundation of China, grant nos. 62173296 and 62003113.

Data Availability Statement: Data sharing is not applicable to this article, as no datasets were generated or analyzed during the current study.

Conflicts of Interest: The authors declare no conflict of interest.

References

1. Giovannetti, V.; Lloyd, S.; Maccone, L. Advances in quantum metrology. *Nat. Photonics* **2011**, *5*, 222–229. [CrossRef]
2. Giovannetti, V.; Lloyd, S.; Maccone, L. Quantum metrology. *Phys. Rev. Lett.* **2006**, *96*, 010401. [CrossRef] [PubMed]
3. Liu, J.; Lu, X.M.; Sun, Z.; Wang, X. Quantum multiparameter metrology with generalized entangled coherent state. *J. Phys. A Math. Theor.* **2016**, *49*, 115302. [CrossRef]
4. Joo, J.; Munro, W.J.; Spiller, T.P. Quantum metrology with entangled coherent states. *Phys. Rev. Lett.* **2011**, *107*, 083601. [CrossRef]
5. Ma, J.; Wang, X.; Sun, C.P.; Nori, F. Quantum spin squeezing. *Phys. Rep.* **2011**, *509*, 89–165. [CrossRef]
6. Tan, Q.S.; Zhang, M.; Chen, Y.; Liao, J.Q.; Liu, J. Generation and storage of spin squeezing via learning-assisted optimal control. *Phys. Rev. A* **2021**, *103*, 032601. [CrossRef]

7. Anisimov, P.M.; Raterman, G.M.; Chiruvelli, A.; Plick, W.N.; Huver, S.D.; Lee, H.; Dowling, J.P. Quantum metrology with two-mode squeezed vacuum: Parity detection beats the Heisenberg limit. *Phys. Rev. Lett.* **2010**, *104*, 103602. [CrossRef]
8. Gazeau, J.P.; Heller, B. Positive-operator valued measure (POVM) quantization. *Axioms* **2014**, *4*, 1–29. [CrossRef]
9. Singal, T.; Maciejewski, F.B.; Oszmaniec, M. Implementation of quantum measurements using classical resources and only a single ancillary qubit. *Npj Quantum Inf.* **2022**, *8*, 1–7. [CrossRef]
10. Caves, C.M. Quantum-mechanical noise in an interferometer. *Phys. Rev. D* **1981**, *23*, 1693–1708. [CrossRef]
11. Liu, J.; Yuan, H. Quantum parameter estimation with optimal control. *Phys. Rev. A* **2017**, *96*, 012117. [CrossRef]
12. Liu, J.; Yuan, H. Control-enhanced multiparameter quantum estimation. *Phys. Rev. A* **2017**, *96*, 042114. [CrossRef]
13. Xu, H.; Li, J.; Liu, L.; Wang, Y.; Yuan, H.; Wang, X. Generalizable control for quantum parameter estimation through reinforcement learning. *Npj Quantum Inf.* **2019**, *5*, 1–8. [CrossRef]
14. Rams, M.M.; Sierant, P.; Dutta, O.; Horodecki, P.; Zakrzewski, J. At the limits of criticality-based quantum metrology: Apparent super-Heisenberg scaling revisited. *Phys. Rev. X* **2018**, *8*, 021022. [CrossRef]
15. Gietka, K.; Metz, F.; Keller, T.; Li, J. Adiabatic critical quantum metrology cannot reach the Heisenberg limit even when shortcuts to adiabaticity are applied. *Quantum* **2021**, *5*, 489. [CrossRef]
16. Hou, Z.; Jin, Y.; Chen, H.; Tang, J.F.; Huang, C.J.; Yuan, H.; Xiang, G.Y.; Li, C.F.; Guo, G.C. "Super-Heisenberg" and Heisenberg Scalings Achieved Simultaneously in the Estimation of a Rotating Field. *Phys. Rev. Lett.* **2021**, *126*, 070503. [CrossRef] [PubMed]
17. Rouchon, P. Models and feedback stabilization of open quantum systems. *arXiv* **2014**, arXiv:1407.7810.
18. Sarlette, A.; Raimond, J.M.; Brune, M.; Rouchon, P. Stabilization of Nonclassical States of the Radiation Field in a Cavity by Reservoir Engineering. *Phys. Rev. Lett.* **2011**, *107*, 010402. [CrossRef]
19. Sarlette, A.; Leghtas, Z.; Brune, M.; Raimond, J.M.; Rouchon, P. Stabilization of Nonclassical States of One-and Two-mode Radiation Fields by Reservoir Engineering. *Phys. Rev. A* **2012**, *86*, 012114. [CrossRef]
20. Cheng, W.; Hou, S.; Wang, Z.; Yi, X. Quantum metrology enhanced by coherence-induced driving in a cavity-QED setup. *Phys. Rev. A* **2019**, *100*, 053825. [CrossRef]
21. Guo, F.; Liu, Y.H.; Daughton, W.; Li, H. Particle acceleration and plasma dynamics during magnetic reconnection in the magnetically dominated regime. *Astrophys. J.* **2015**, *806*, 167. [CrossRef]
22. Miao, Z.; Sarlette, A. Discrete-time reservoir engineering with entangled bath and stabilising squeezed states. *Quantum Sci. Technol.* **2017**, *2*, 034013. [CrossRef]
23. Miao, Z.; Chen, Y.; Yuan, H. Is entanglement necessary in the reservoir input? In Proceedings of the 2019 IEEE 58th Conference on Decision and Control, Nice, France, 11–13 December 2019; pp. 407–412.
24. Jaekel, M.T.; Reynaud, S. Quantum limits in interferometric measurements. *Europhys. Lett.* **1990**, *13*, 301. [CrossRef]
25. Xie, Y.M.; Lu, Y.S.; Weng, C.X.; Cao, X.Y.; Jia, Z.Y.; Bao, Y.; Wang, Y.; Fu, Y.; Yin, H.L.; Chen, Z.B. Breaking the rate-loss bound of quantum key distribution with asynchronous two-photon interference. *PRX Quantum* **2022**, *3*, 020315. [CrossRef]
26. Gu, J.; Cao, X.Y.; Fu, Y.; He, Z.W.; Yin, Z.J.; Yin, H.L.; Chen, Z.B. Experimental measurement-device-independent type quantum key distribution with flawed and correlated sources. *Sci. Bull.* **2022**, *67*, 2167–2175. [CrossRef] [PubMed]
27. Yin, H.L.; Fu, Y.; Li, C.L.; Weng, C.X.; Li, B.H.; Gu, J.; Lu, Y.S.; Huang, S.; Chen, Z.B. Experimental quantum secure network with digital signatures and encryption. *arXiv* **2021**, arXiv:2107.14089.
28. Zhou, M.G.; Cao, X.Y.; Lu, Y.S.; Wang, Y.; Bao, Y.; Jia, Z.Y.; Fu, Y.; Yin, H.L.; Chen, Z.B. Experimental quantum advantage with quantum coupon collector. *Research* **2022**, *2022*, 9798679. [CrossRef] [PubMed]
29. Helstrom, C.W. Quantum detection and estimation theory. *J. Stat. Phys.* **1969**, *1*, 231–252. [CrossRef]
30. Braunstein, S.L.; Caves, C.M. Statistical distance and the geometry of quantum states. *Phys. Rev. Lett.* **1994**, *72*, 3439. [CrossRef]
31. Demkowicz-Dobrzański, R.; Maccone, L. Using entanglement against noise in quantum metrology. *Phys. Rev. Lett.* **2014**, *113*, 250801. [CrossRef] [PubMed]
32. Liang, Y.C.; Yeh, Y.H.; Mendonça, P.E.; Teh, R.Y.; Reid, M.D.; Drummond, P.D. Quantum fidelity measures for mixed states. *Rep. Prog. Phys.* **2019**, *82*, 076001. [CrossRef] [PubMed]